MedChemComm

Journal Name

MedChemComm Accepted Manuscript

ARTICLE

Synthesis and Preclinical Evaluation of a Novel, Selective ^{111}In-labelled Aminoproline-RGD-peptide For Non-invasive Melanoma Tumor Imaging†

Andrea Sartori,[a] Francesca Bianchini,[b,c] Silvia Migliari,[d] Paola Burreddu,[e] Claudio Curti,[a] Federica Vacondio,[a] Daniela Arosio,[f] Livia Ruffini,[d] Gloria Rassu,[e] Lido Calorini,[b] Alberto Pupi,[b,c] Franca Zanardi[a] and Lucia Battistini*[a]

In recent years, many efforts have been addressed to develop new imaging techniques enabling the early diagnosis and non-invasive monitoring in primary tumors and metastases. Among the integrin family, $\alpha_v\beta_3$ and $\alpha_5\beta_1$ receptors have been characterized as prototypic markers of angiogenic tumor associated-endothelial cells and their overexpression in tumor cells has been correlated to the progression of various tumor types such as melanoma. Herein we report the synthesis, characterization and preclinical evaluation of a ^{111}In-labelled DOTA-conjugate embodying a cyclic aminoproline-RGD-peptide motif as a competent $\alpha_v\beta_3$ integrin ligand, to be used as radiotracer in preclinical models of human melanoma. Practical and efficient chemical and radiochemical syntheses were set up; in vitro stability and hydrophilicity of a cold c(AmpRGD)-DOTA-conjugate were demonstrated; binding affinities toward isolated $\alpha_v\beta_3/\alpha_5\beta_1$ receptors were assayed and inhibition of cell adhesion to vitronectin and fibronectin was tested in human melanoma and endothelial progenitor cell lines. The anti-angiogenic activity of peptide conjugates was also tested and assessed in vitro by tubulogenesis assays. The in vivo biodistribution SPECT/CT studies in healthy mice revealed high renal uptake at earlier observation times (30 min – 4 h p.i.) and complete clearance from kidney at 48 h p.i.; displacement experiments in human melanoma xenografts confirmed the $\alpha_v\beta_3/\alpha_5\beta_1$ integrin specificity of tumor uptake suggesting the ^{111}In-labelled c(AmpRGD)-DOTA bioconjugate as a promising starting point in the search for new SPECT-imaging small-molecular probes for non-invasive visualization of tumor angiogenesis, human melanoma and other $\alpha_v\beta_3/\alpha_5\beta_1$-positive tumors.

Introduction

Angiogenesis, defined as the sprouting of new blood vessels from pre-existing vasculature represents the normal response to hypoxic conditions and is tightly regulated by the balance between pro- and anti-angiogenic factors.[1] In pathological conditions including thrombosis, immune dysfunction, inflammation and cancer, this delicate balance is dysregulated. During cancer progression, formation of new vascular network is essential for cancer development and metastatic dissemination,[2] and recently it has become evident the role of circulating bone marrow-derived endothelial progenitor cells (EPC) in tumor-induced neovascularization.[3]

Among skin cancers, melanoma is one of the most aggressive tumors with high angiogenic and metastatic potential, whose early diagnosis is crucial for patient survival. Current imaging modalities used for malignant melanoma staging include positron emission tomography/computed tomography (PET/CT) based on [18F]-fluorodeoxyglucose ([18F]-FDG) detection, but its sensitivity is not sufficient for very early diagnosis of disseminated metastases. Thus, highly selective imaging probes targeting specific biomarkers of melanoma cells and surrounding endothelial cells are still urgent and topical.[4,5]

Since the early studies it became clear that cell adhesion molecules, in particular integrins, play a crucial regulatory role in tumor vascular remodelling and angiogenesis.[6-9] Integrins are members of a membrane adhesion receptor family containing two different non-covalently associated subunits (α and β). Among the many different classes of integrins, the $\alpha_v\beta_3$ and $\alpha_5\beta_1$ subsets are recognized as key factors in neovascularization and progression of various tumor types including melanoma. Integrins $\alpha_v\beta_3$ and $\alpha_5\beta_1$, among many others, recognize the tripeptide Arg-Gly-Asp (RGD) sequence within different types of ligands present in the extracellular matrices, such as fibronectin (FN) and

[a] Dipartimento di Farmacia, Università degli Studi di Parma, Parma 43124, Italy.
[b] Dipartimento di Scienze Biomediche, Sperimentali e Cliniche, "Mario Serio" Università degli Studi di Firenze, Firenze 50134, Italy.
[c] Centro Interdipartimentale per lo Sviluppo Preclinico dell'Imaging Molecolare (CISPIM), Università degli Studi di Firenze, Firenze 50134, Italy.
[d] Dipartimento di Medicina Nucleare, Azienda Ospedaliero-Universitaria di Parma, Parma 43126, Italy.
[e] Istituto di Chimica Biomolecolare, Consiglio Nazionale delle Ricerche, Li Punti Sassari 07100, Italy.
[f] Istituto di Scienze e Tecnologie Molecolari, Consiglio Nazionale delle Ricerche, Milano 20133, Italy.
†Electronic Supplementary Information (ESI) available: Detailed procedures for chemistry, radiochemistry, in vitro and in vivo experiments. See DOI: 10.1039/x0xx00000x
*Correspondence to: Lucia Battistini – Dipartimento di Farmacia – Università degli Studi di Parma – e-mail: lucia.battistini@unipr.it

vitronectin (VN), exhibiting different binding affinities and specificity profiles.[10-12] Over the past two decades, RGD-recognizing integrins have been the object of intense investigations in the field of targeted therapies, as well as in the domain of targeted tumor imaging. A great deal of work has been devoted to the synthesis and development of specific and high-affinity small molecular integrin ligands including peptides, semipeptides and peptidomimetics bearing or mimicking the RGD-sequence.[13-21] The renowned cyclic pentapeptide c(RGDf[N-Me]V) (Cilengitide)[13] developed by Kessler and coworkers represents a milestone in this domain. Conjugable Cilengitide analogues (cRGDfK, cRGDyK) have been exploited as targeting moieties to consign cytotoxic and/or imaging agents to the tumor tissue under the shape of either mono-, multimeric covalent conjugates, or nanosized supramolecular entities.[14,22-24]

Molecular imaging techniques have witnessed a rapidly growing interest in recent years since they enable non-invasive visualization and characterisation of physiological or pathological processes at the molecular and cellular levels in living systems. In particular, due to favourable features of nuclear imaging approaches, including PET and SPECT modalities, several radionuclide-based probes have been successfully translated from preclinical to clinical settings for assessing pathological angiogenesis, preventing cancer cells dissemination, monitoring and validating therapies, optimising dose regimens, flanking surgery, in line with the emerging concept of "personalized medicine".[25-31]

Despite notable results achieved in the search for new and effective small molecular RGD-based radiotracers for both PET and SPECT imaging of integrin expression, most attention has been paid to both selection of the active unit to be attached and design of the linker moiety modulating the pharmacokinetic properties of new constructs.[32-34] However, minor efforts have been devoted toward the exploitation of high-affinity RGD-binders alternative to the reference cyclopeptide cRGDfK. The development of new RGD-based peptidomimetic ligands could be of relevant interest since their unexplored physicochemical properties and ligand competence could be nicely exploited to broaden and complement the palette of existing integrin-directed bioconjugates.[14,16-21]

c(AmpRGD)-NH$_2$ (**1**)

^{111}In-DOTA-c(AmpRGD) (^{111}**In-2**)
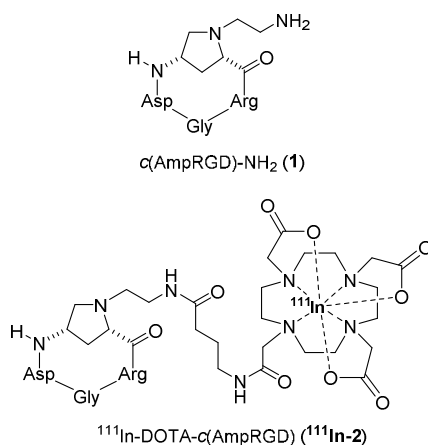
Fig. 1 Structure of Amp-based RGD-semipeptide **1** and its radiolabelled DOTA-conjugate ^{111}**In-2**.

Along this line, we propose here the synthesis and preclinical evaluation of a novel ^{111}In-labelled bioconjugate ^{111}**In-2** exploiting the γ-aminoproline-RGD-based cyclotetrapeptide **1** as clever "navigator" unit to target the $\alpha_V\beta_3$ and $\alpha_5\beta_1$ integrins (Figure 1). Recently we described the synthesis of a new class of cyclic semipeptides containing the 4-aminoproline scaffold (Amp) grafted onto the tripeptide RGD, which showed low nanomolar binding affinity toward the isolated $\alpha_V\beta_3$ and $\alpha_V\beta_5$ integrin receptors.[35] When conjugated with various sterically demanding ancillary active moieties (e.g. paclitaxel, fluorescein, 1,4,7,10-tetraazacyclododecane-1,4,7,10-tetra-acetic acid [DOTA], and phospholipid units) these ligands maintained their binding capability, while showing, in some instances, remarkably increased $\alpha_V\beta_3$ vs $\alpha_V\beta_5$ selectivity.[17,21,36] As an evolution of our previous work, in this study we aimed at 1) improving the synthetic procedure to access the c(AmpRGD)-DOTA conjugate **2** in an economic and high-yielding way; 2) setting up practical and efficient radiolabelling procedure with ^{111}In radioisotope; 3) testing in vitro the targeting capability towards human melanoma cell lines and circulating EPCs overexpressing $\alpha_V\beta_3$ and $\alpha_5\beta_1$ integrins; 4) evaluating in vitro the anti-angiogenic capability of the conjugates; 5) evaluating in vivo the ^{111}In-labelled DOTA-conjugate ^{111}**In-2** as a single photon emission computed tomography (SPECT) tracer in animal models of human melanoma.

Results

Chemistry and Radiochemistry

Synthesis of cyclopeptide 1 and DOTA-conjugate 2 The protected c(AmpRGD)-NH$_2$ **5** to be used in the conjugation step with DOTA derivative **6** (Scheme 1) was prepared by using standard Fmoc-solid phase peptide synthesis (SPPS) starting from γ-aminoproline scaffold **4**, that in turn was synthesized from commercial L-*trans*-hydroxyproline (**3**) (13 chemical steps, 11% overall yield). Acidic removal of side chain protecting groups within **5** followed by semi-preparative RP-HPLC purification and lyophilisation afforded amino-derivative **1**, which served as the reference compound in biological assays. To advance the synthesis of conjugate **2**, cyclopeptide **5** was coupled to the protected chelating unit DOTA **6** through a four carbon-long amide linker under standard peptide coupling conditions. The final deblocking of the side chain protecting groups followed by HPLC purification afforded conjugate **2** in 60% yield over two steps. Compound **2** was characterized by ESI-MS, mono- and bidimensional NMR, and all data were consistent with the proposed formula (see ESI for details)

Synthesis and stability of cold In-DOTA-conjugate In-2 In order to evaluate the stability of In-DOTA chelate compound **In-2**, a cold analogue of the radiolabelled candidate, was prepared. Cold **In-2** was incubated in rat and human plasma and HPLC-ESI-MS/MS analysis was performed to evaluate the stability of the compound at different time points, up to 6 h incubation, at 37 °C. The HPLC-ESI-MS/MS chromatogram of plasma samples revealed one major peak, corresponding to the double charged ion [M+2H]$^{2+}$ at m/z = 534.1 with identical shape and retention time (R_t = 4.15-4.20 min) as the control peak in the absence of plasma (see ESI, Figure S1). Compound **In-2** remained stable in both rat and human plasma and was recovered unmodified at 6 hours as percentages of 102.2 ± 8.2% and 97.0 ± 8.3% (mean ± SD, n=3), respectively. No peak

corresponding to the In-free ligand **2** (R_t = 5.2 min) was observed under the same incubation conditions (see ESI, Figure S2).

Scheme 1 Synthesis of c(AmpRGD)-NH$_2$ **1** and its DOTA-conjugate **2**[a]
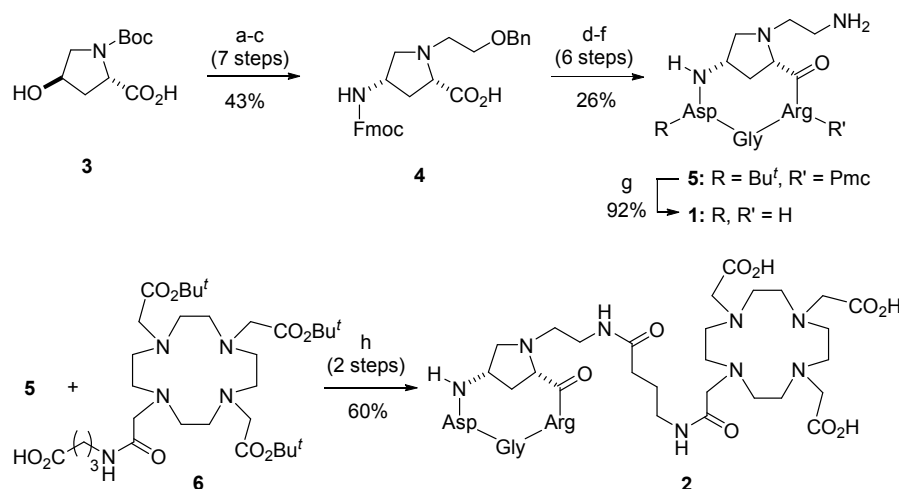
^{a}Reagents and conditions: a) DIC, Bu^{t}OH, CuCl, DCM, 3 days (87%); DEAD, PPh$_3$, DPPA, THF, 0 °C to rt (91%); b) H$_2$, Pd/C, MeOH (99%); FmocOSu, aq Na$_2$CO$_3$, THF (74%); c) Bu^{t}OAc, MeSO$_3$H, DCM, 3 days (87%); CHOCH$_2$OBn, NaBH(OAc)$_3$, DCE, rt (93%); TFA, anisole (91%); d) SPPS: 2-Chlorotrityl-Gly-H resin; Fmoc-Arg(Pmc)-OH; Fmoc-Asp(Bu^t)-OH; coupling system: DEPBT, DIEA, DMF; Fmoc removal: 20% piperidine/DMF; cleavage: AcOH/TFE/DCM (1:1:3) (80%); e) HATU, HOAt, collidine, DMF (medium dilution, 3.0 mM) (64%); f) 50 psi H$_2$, Pd/C, MeOH, HCO$_2$H (80%); MsCl, Et$_3$N, CH$_3$CN; then NaN$_3$, DMF, reflux (70%, 2 steps); H$_2$, Pd/C, EtOH (89%); g) TFA/TIS/H$_2$O (92%); h) HBTU, DIEA, DCM (68%); TFA/TIS/H$_2$O (89%) (see abbreviations in ESI).

*Determination of distribution coefficient (Log $D_{oct,7.4}$) of **In-2*** The measured n-octanol/buffer distribution coefficient (Log $D_{oct,7.4}$) for **In-2** was calculated as the mean of three independent measurements ± SD and resulted to be −3.20 ± 0.12, thus demonstrating the predominant hydrophilic character of In-DOTA-conjugate.

Radiolabelling ^{111}In-DOTA-c(AmpRGD) **^{111}In-2** was prepared by reacting DOTA-conjugate **2**, pre-dissolved in NH$_4$OAc buffer, with ^{111}InCl$_3$ in 0.05 M HCl. In order to set up the optimal labelling conditions, parameters such as In:ligand ratio, ligand concentration, temperature, final pH and reaction time were carefully evaluated and radiochemical purity (RCP) was assessed by radio-TLC.
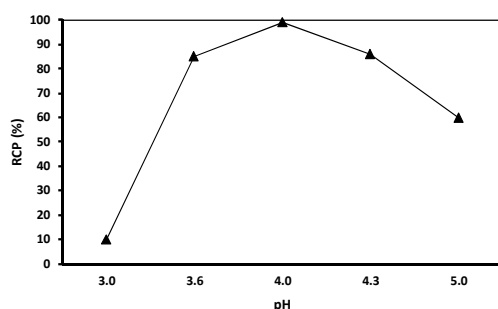

Fig. 2 Dependence of RCP (%) on the final pH of the reaction mixture (In:ligand ratio 1:6.2, ligand concentration 0.02 mM).

The best result was obtained by reacting compound **2** (2.39 nmol) with ^{111}InCl$_3$ (40 MBq) to a final 1:6.2 In:ligand ratio, ligand concentration 0.02 mM and pH 4.0. The RCP resulted >99% without further purification and the specific activity was 16.7 MBq/nmol (0.48 mCi/µg) (see ESI, Figure S3). To minimize the interference of non-labelled ligand in the receptor recognition event, the In:ligand ratio was lowered to 1:3.1. Thus, DOTA-conjugate **2** (1.19 nmol) was reacted with ^{111}InCl$_3$ (40 MBq) affording a good >93% RCP without further purification and a specific activity of 33.6 MBq/nmol (0.96 mCi/µg), which was judged viable for following in vivo studies (see ESI, Figure S4). Crucial to the success of the labelling procedure was the setting of the reaction mixture pH: when pH was adjusted to 5.0, only 60% RCP could be obtained, lowering the pH to 4.3 RCP raised to 86%, while the highest purity was reached when the pH was exactly 4.0 (Figure 2).

Biology

Solid phase receptor binding assay The ability of cold conjugate **In-2** to bind to human $\alpha_v\beta_3$ and $\alpha_5\beta_1$ integrin receptors was evaluated in vitro by competitive binding assays using biotinylated VN and FN (Table 1). To better examine the impact of DOTA appendage and metal chelation on binding capability, the results were compared to those obtained for the unconjugated counterpart c(AmpRGD)-NH$_2$ **1**, non-metalated compound **2** and commercial ligand c(RGDfV). Both DOTA-conjugates **2** and **In-2** displayed binding affinities toward both integrin receptors in the nanomolar range, with a preference for $\alpha_v\beta_3$ receptor (one-digit nanomolar binding affinities). The data were comparable to those of reference compounds **1** and c(RGDfV).

Journal Name

ARTICLE
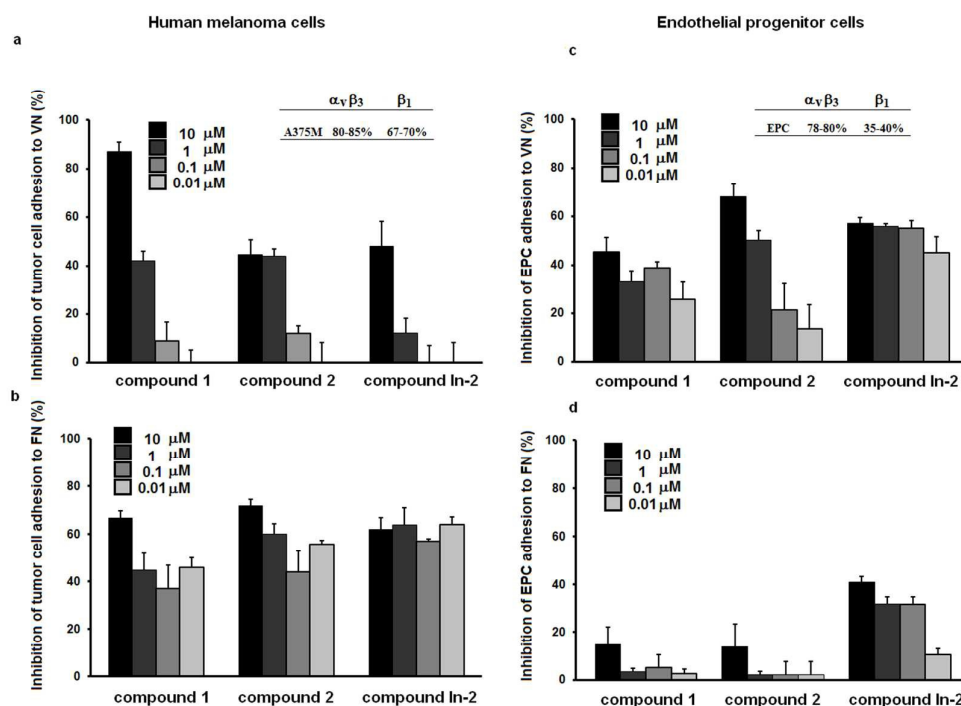
Fig. 3 Adhesion inhibition of A375M melanoma cells (panels a, b) and EPCs (panels c, d) to VN and FN in the presence of compounds **1**, **2** and **In-2**. Top inserts indicate the percentage of integrin subunit expression in human melanoma cells and EPCs. The inhibitory activity was calculated as percentage of cell adhesion to VN and FN in untreated cells and was expressed as mean ± SD. Experiments were conducted in triplicate.

Table 1 Inhibition of biotinylated VN and FN binding to $\alpha_V\beta_3$ and $\alpha_5\beta_1$ receptors, respectively[a]

Compound	IC$_{50}$ (nM) ± SD for $\alpha_V\beta_3$	IC$_{50}$ (nM) ± SD for $\alpha_5\beta_1$
1	6.1±1.6[b]	151.6±67.6
2	6.9±0.6[b]	123.4±65.8
cold **In-2**	2.8±0.4	101.2±26.0
c(RGDfV)	3.2±1.3[b]	166.0±28.0

[a]IC$_{50}$ values were calculated as the concentration of compound required for 50% inhibition of biotinylated VN and FN binding as estimated by the Prism GraphPad program. All values are the mean (± SD) of triplicate determinations.
[b]Ref. 36

Cell biology assays Both A375M human melanoma cells and EPCs were used to evaluate the ability of compound **In-2** to inhibit cell adhesion to RGD-containing substrates VN and FN. For comparison purposes, compounds **1** and **2** were also evaluated in the same assays. Both A375M cells and EPCs express integrin subunits α_V, β_3 and β_1, as revealed by flow cytometric analysis, with EPC expressing β_1 at lower levels (Figure 3, top inserts; see ESI, Figure S5).

The adhesion inhibitory assays were performed in the presence of 2 mmol/L MnCl$_2$ to switch integrins to activated form and tested compounds were used at final concentrations of 10, 1.0, 0.1 and 0.01 μM, respectively. Figure 3 (panel a) shows A375M cell adhesion to VN in the presence of compounds **1**, **2** and **In-2**: compound **1** at 10 μM concentration strongly inhibited cell adhesion and this effect was clearly dose-dependent; compounds **2** and **In-2** showed similar inhibitory trend but lower activity as compared to compound **1**. On the other hand, melanoma cells adhesion to FN (panel b) was efficiently suppressed even at lower concentrations for all tested compounds. Compounds **1** and **2** showed dose-dependent inhibitory effect on EPC adhesion to VN (panel c), while inhibitory effect of **In-2** remained quite relevant at the different concentrations tested. EPC adhesion to FN was inhibited in a dose-dependent manner by chelate **In-2**, while compounds **1** and **2** showed to be ineffective (panel d).
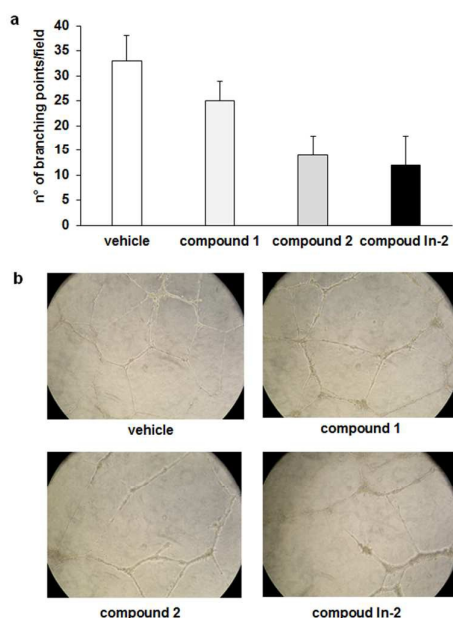
Fig. 4 In vitro tubulogenesis in EPCs grown for 18 h in the presence of compounds **1**, **2**, **In-2** (10 μM). a) Histograms refer to the relative quantification and are expressed as mean value ± SD. *P <0.05, significantly different from control. b) Representative images of different treatments. Experiments were conducted in triplicate.

In vitro capillary network formation To evaluate the anti-angiogenic activity of compounds **1**, **2** and **In-2** in vitro, the ability of these peptides to interfere with EPC in organizing capillary network was determined. Cells were seeded on Matrigel layers and incubated for 18 h in the presence of the peptides at 10 μM concentration. The quantification was performed by measuring the percentage of node connected by capillary projections (branching points), assuming the control as 100%. All tested compounds significantly reduced the number of branching points (Figure 4).

In vivo studies

All experimental procedures involving animals were performed in accordance with national guidelines, approved by the Ethical committee of the Animal Welfare Office of the Italian Work Ministry and conformed to the legal mandates and Italian guidelines for the care and maintenance of laboratory animals.

Biodistribution studies Biodistribution studies were performed in male CD1 nu/nu healthy mice to evaluate radioactivity distribution at 30, 120 min and 4 h post injection. Absolute activity concentration in the target organ (*AACt*) was analyzed in heart, lungs, liver, gallbladder, spleen, pancreas, stomach, small and large intestine, kidneys, and urinary bladder; in particular for the intestine, *AACt* was assessed at the site showing the highest tracer uptake. Final *AACt* data for each organ were normalized to the activity in a surrounding region and reported as *nACt*; contralateral muscle tissue was selected as reference tissue (see ESI). Figure 5 illustrates SPECT/CT images of a representative mouse administered with [111]In-2 (2.81 MBq): SPECT/CT co-registered images show coronal slices taken at different levels of the mouse body (panel a), and histograms account for radiotracer uptake in different organs (panel b).

The biodistribution studies pointed out a rapid blood clearance as suggested by reduced tracer activity in lungs and heart at 30 min post-injection; the urinary bladder, due to its rapid rate of filling and emptying, was not included in the chart. Interestingly, liver, gallbladder, small and large intestine, members of the enterohepatic excretion cycle, were only partially involved in the excretion process, as compared to kidneys. The stomach resulted marginally interested in the excretion process within the first 30 min of observation, while spleen and pancreas resulted not involved in the elimination process. The latter acquisition taken at 48 h p.i. revealed that the tracer was completely cleared from kidneys and other organs (see ESI, Figure S6).

Human melanoma xenografts uptake Saturation experiments (SE) and displacement experiments (DE) were performed in human melanoma xenografted mice to evaluate tumor targeting capability and specificity of tumor uptake (Figure 6). SE were performed at 30, 60 and 120 min p.i. in accordance with the rapid biological half-lives of DOTA-conjugated small peptides[37] and according to data from biodistribution studies. Radiotracer uptake was measured in tumor tissue and data were normalized to muscle activity as background activity and expressed as *nACt* (see ESI). SPECT/CT images in Figure 6 (panel b) show radioligand tumor uptake in the absence (saturation) and in the presence (displacement) of an excess of cold ligand **2**; uptake quantification data (panels a and c) are presented as *nACt* in tumor tissue. Uptake of radioligand [111]In-2 in tumor tissue at 30 min was 11.9±1.4 (*nACt*), while resulting nearly halved at 60 min (5.3±0.7). Tumor uptake in displacement experiments was significantly reduced (83.4% blockage) as compared to saturation experiments (p=0.032), thus confirming the specificity of integrin-mediated radiotracer tumor uptake.

Discussion

Based on the Cilengitide-like cyclopentapeptides c(RGDfK), c(RGDyK), and disulphide-bridged RGD-scaffold RGD-4C,[14] a wide library of molecular entities has been tested in the past decade as radiotracers, which differed from each other by the nature of the radionuclide, chelating unit, linker moiety, and ancillary appendages able to modulate the overall pharmacokinetic properties. Among the few representative RGD tracers advanced to in-depth clinical evaluation, the glycosylated ^{18}F-galacto-RGD probe offered a viable strategy for non-invasive mapping of tumor vascular $\alpha_V\beta_3$ expression and detection of primary malignant tumors including melanoma, breast cancer, glioblastoma multiforme, renal cell carcinoma and colorectal carcinoma.[38] However, a lower detection rate for lymph nodes and distant metastases, as well as no clear differentiation between benign and malignant lesions were observed for this tracer. Given the open questions in the field of selective non-invasive visualization of pathological angiogenesis and malignant metastatic tumors, the search of new, structurally modulable molecular probes is far from being covered.

Drawing inspiration from previous work by our laboratories on the exploitation of aminoproline-based RGD-cyclopeptides as clever systems targeting $\alpha_V\beta_3$ integrin,[17,21,36] we selected the RGD-based cyclopeptide c(AmpRGD)-NH₂ **1** as the addressing unit to deliver an imaging-effective radionuclide to angiogenic vascular endothelium and melanoma tumor tissues.

Journal Name
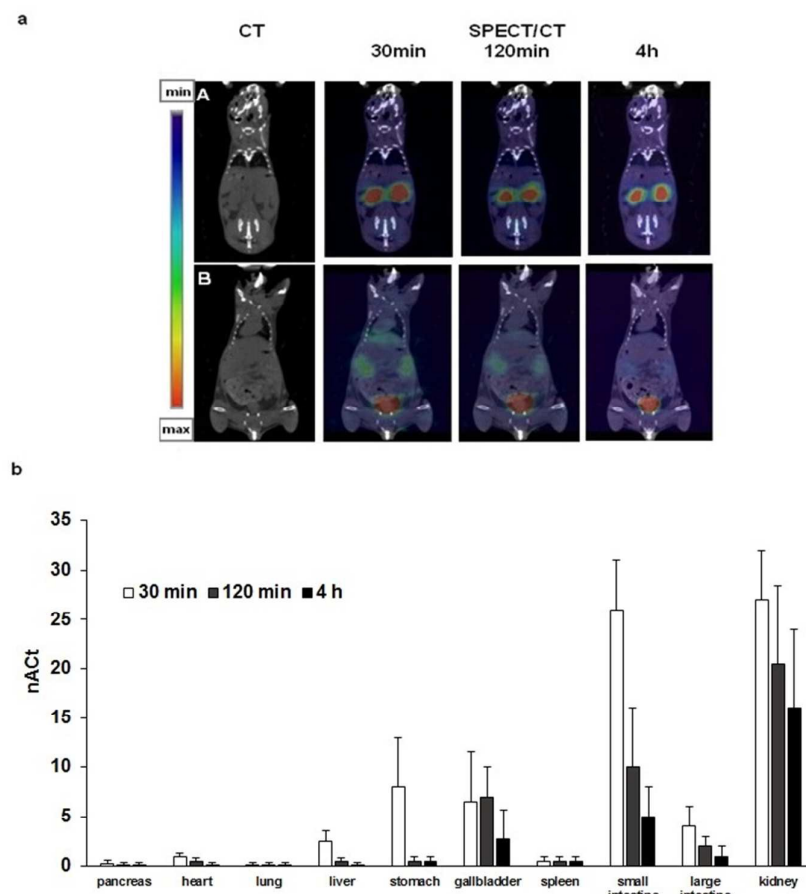
Fig. 5 [111]**In-2** biodistribution in healthy mice. a) SPECT/CT images at 30, 120 min and 4 h p.i. taken at different sections of mouse body (coronal slices A and B). b) Biodistribution data referring to [111]**In-2** radiotracer in different organs. Radiotracer uptake efficiency was expressed as *nACt* ± SD (n=3).

In this study, optimization of the previously described synthesis of aminoproline-based DOTA-conjugate **2** was firstly addressed (Scheme 1; see ESI, Schemes S1 and S2);[35,36] the overall synthetic sequence was shortened from 20 to 15 linear steps starting from a commercial and inexpensive protected L-hydroxyproline precursor. The SPPS protocol was improved from 47% to a good 80% yield for the peptide construction by judicious choice of amino acid side-chain protecting groups, coupling reagents, and pre-loaded resin. Also, optimization of parameters critical for the macrocyclization step and elaboration of the benzyloxyethyl chain was carried out, including careful evaluation of solvent polarity, reaction mixture concentration, and reaction temperature.

A cold **In-2** conjugate was then prepared to evaluate stability and distribution coefficient (Log $D_{oct,7.4}$) of the metal-chelated derivative. The **In-2** complex was stable for >6 h without any decomposition in the presence of both human and rat plasma, as well as in saline solution (pH 7.4) (see ESI, Figures S1 and S2). The Log *D* resulted −3.20 in accordance with the predominant hydrophilic character of the conjugate, which ultimately could account for the rapid blood clearance and preferential renal excretion (vide infra), as observed for other radiolabelled peptides.[37]

The binding affinity of compounds **1**, **2** and **In-2** toward $\alpha_V\beta_3/\alpha_5\beta_1$ integrins was evaluated in vitro by competitive displacement assays on isolated integrin receptors. The involvement of $\alpha_V\beta_3$ and $\alpha_5\beta_1$ integrins in tumor angiogenesis is well documented,[7-10] although their intertwining functions are still far from being completely elucidated.[11-12] While a few interesting studies exist about the discovery of $\alpha_V\beta_3$- or $\alpha_5\beta_1$-selective ligands,[39] emerging evidences point to emphasize the merits of dual $\alpha_V\beta_3/\alpha_5\beta_1$-addressed ligands as useful targeting tools to tumor-related tissues where both receptors are contemporarily involved.[40] The IC$_{50}$ displayed by all

tested compounds toward both receptors were in the nanomolar range, with a preference for the $\alpha_v\beta_3$ receptor (Table 1). The notable ligand competence of conjugate **2** and chelate **In-2** toward these integrin receptors demonstrates that conjugation with bulky DOTA appendage and metal-chelation do not impair the binding capabilities of these AmpRGD cyclopeptides, a valuable feature in the search for new visualizing probes directed to tumor cells and microenvironment tumor cells.

To confirm the biological activity of In-DOTA conjugate on integrin receptors, the ability of **In-2** to inhibit A375M human melanoma cell and EPC adhesion to VN and FN was evaluated and compared to that of the parent cyclopeptide **1** and metal-free ligand **2** (Figure 3). All the assayed ligands inhibited the melanoma cell adhesion to FN in nanomolar concentrations, and efficient inhibitory activity of EPC adhesion to VN was found as well. On the other hand, **In-2** resulted more efficient in inhibiting EPC adhesion to FN as compared to its parent compounds. Interestingly, the chelation of indium metal positively influences the activity of **In-2** on cell adhesion to both natural integrin ligands in line with the binding results on isolated receptors. While the actual role of the chelated metal in the binding event is hardly predictable, it is plausible that the indium metal influences the overall shape and physicochemical properties of the molecule thereby modulating the binding affinity. Human melanoma cells and EPCs were demonstrated to express different levels of $\alpha_v\beta_3$ and $\alpha_5\beta_1$ receptors and, unexpectedly, this expression pattern does not linearly correlate with inhibition of cell adhesion exerted by **In-2**. Additional factors affecting the cell membrane microenvironment in which integrin are expressed could be invoked to rationalize this result. The pattern distribution and co-localization of integrins, their exocytic-endocytic cycling, the mutual influence of $\alpha_v\beta_3$ and $\alpha_5\beta_1$ through complex cross-talk signalling events, as well as the presence of different downstream accessory proteins,[41] should all be taken into consideration.[11,12,42]

Tubulogenesis assays (Figure 4) were set up to test the ability of these RGD conjugates to interfere with EPC tube formation on Matrigel layers: **In-2** and its non-chelated counterpart **2** significantly reduced capillary network formation by EPC at 10 μM concentration.

A practical and efficient radiolabelling procedure was set up. The careful selection of radiolabelling parameters, such as In:ligand ratio, temperature and reaction time, ligand concentration and, most of all, pH of the reaction mixture, resulted in high RCP and specific activity (Figure 2). With an In:ligand ratio of 1:6.2, a >99% RCP (16.7 MBq/nmol specific activity) was reached, while lowering the peptide amount to 1:3.1 In:ligand ratio, resulted in a good >93% RCP (33.6 MBq/nmol specific activity), which was judged an optimal balance between overall efficiency, indium:peptide ratio and practicality (see ESI, Figures S3 and S4). The short radiosynthesis time (20 min) and high specific activity of tracer [111]**In-2** made radio-HPLC purification unnecessary and rendered this procedure attractive in view of possible future translation to clinics.

Molecular imaging studies represent a unique opportunity to obtain longitudinal biodistribution data avoiding ex vivo investigations, corroborating data themselves and reducing the number of mice to be sacrificed for necropsy, according to the principles of the 3Rs. Therefore, biodistribution and tumor uptake data are not expressed as %ID/g of tissue, but are reported as normalized activity concentration in the target organ/tumor (*nACt*), providing a sound modality to evaluate the "binding potential" in compartmental systems at the equilibrium. This method is usually applied in molecular imaging both in preclinical and clinical practice.

Biodistribution studies in healthy mice administered with [111]**In-2** showed high renal uptake, as expected, due to tubular reabsorption and prolonged renal retention (Figure 5); these megalin-mediated processes have been observed for other radiolabelled peptides used for radiotherapeutic purposes and have been correlated to nephrotoxicity risk.[43] Of note, the observed renal uptake of [111]**In-2** was limited to the initial period of monitoring (30 min – 4 h) and completely cleared at latter acquisition (48 h p.i.; see ESI, Figure S6), accounting for a reduced risk of nephrotoxicity for this compound.

Saturation experiments were performed in immunodeficient mice in order to visualize grafted tumors, and receptor-blocking experiments (displacement experiments) were performed in the same animals to evaluate the $\alpha_v\beta_3/\alpha_5\beta_1$ integrin specificity of labelled conjugate [111]**In-2**. Good visualization of the implanted tumors was obtained with a 11.9±1.4 tumor uptake (*nACt*) at 30 min (Figure 6). A further acquisition at 60 min showed tumor retention nearly halved.
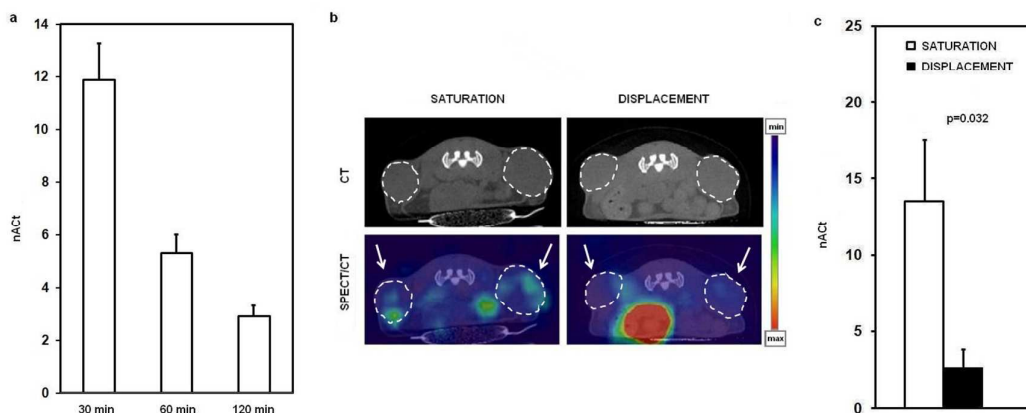
Fig. 6 [111]**In-2** saturation and displacement experiments. a) [111]**In-2** tumor uptake at 30, 60 and 120 min p.i. in human melanoma xenografts. b) SPECT/CT images of SE and DE at 30 min p.i. in a human melanoma xenografted representative mouse bearing two tumor implants in the left and right flank (*arrows*). c) SE and DE at 30 min p.i.. *nACt* in tumor tissue was expressed as mean ± SD (n=3).

The anticipative injection of excess of non-radioactive compound **2** significantly reduced the tumor uptake at 30 min, thus minimizing the unspecific radioligand accumulation in tumor tissues. The preliminary results herein described concerning the tumor visualization and radioligand uptake are in line with previously reported studies on similar ^{111}In-labelled RGD ligands,[44-46] holding promise for the development of optimized radiotracer compounds.

Conclusions

The promising results from in vitro assays displayed by the metal-chelate **In-2** – including the high binding affinities for $\alpha_v\beta_3$ and $\alpha_5\beta_1$ integrin receptors and the inhibitory effects on EPC and human melanoma cell adhesion to VN and FN – together with the practical and highly efficient radiosynthesis protocol, render this integrin binder a versatile probe worth to be further investigated. The preliminary biodistribution data and in vivo imaging studies demonstrated good integrin-mediated tumor targeting capability and tumor uptake of the radiolabelled AmpRGD peptide [111]**In-2**, accompanied by short retention time and rapid blood clearance. We envisage tailoring bioconjugate analogues of [111]**In-2** (e.g. by inserting PEG or polyglycine spacers as the linker moiety associated to alternative chelating unit/radionuclide couples) as an attractive perspective to meet improved biodistribution properties, with the ultimate goal of adding such ^{111}In-DOTA-c(AmpRGD) analogues in the toolkit of currently available RGD radiotracers.

Acknowledgements

Notes

The authors declare no conflict of interest.

References

1   J. Folkman, *Curr. Mol. Med.*, 2003, **3**, 643–651.
2   S.A. Weis, D.A. Cheres, *Nat. Med.*, 2011, **17**, 1359–1370.
3   M. Aghi, E.A. Chiocca, *Mol. Ther.*, 2005, **12**, 994–1005.
4   C. Garbe, T.K. Eigentler, U. Keilholz, A. Hauschild, J.M. Kirkwood, *Oncologist*, 2011, **16**, 5–24.
5   H. Minn, P. Vihinen, *J. Nucl. Med.*, 2011, **52**, 5–7.
6   A.R. Ramjaun, K. Hodivala-Dilke, *Int. J. Biochem. Cell Biol.*, 2009, **41**, 521–530.
7   J.S. Desgrosellier, D.A. Cheresh, *Nat. Rev. Cancer*, 2010, **10**, 9–22.
8   S.L. Goodman, M. Picard, *Trends Pharmacol. Sci.*, 2012, **33**, 405–412.
9   D. Cox, M. Brennan, N. Moran, *Nat. Rev. Drug Discov.*, 2010, **9**, 804–820.
10 C.J. Avraamides, B. Garmy-Susini, J.A. Varner, *Nat. Rev. Cancer*, 2008, **8**, 604–617.
11 S. Kim, M. Harris, J.A. Varner, *J. Biol. Chem.*, 2000, **43**, 33920–33928.
12 A. Stachurska, J. Elbanowski , H.M. Kowalczyńska, *Cell Biol. Int.*, 2012, **36**, 883–892.
13 C. Mas-Moruno, F. Rechenmacher, H. Kessler, *Anti-Cancer Agents Med. Chem.*, 2010, **10**, 753–768.
14 L. Auzzas, F. Zanardi, L. Battistini, P. Burreddu, P. Carta, G. Rassu, C. Curti, G. Casiraghi, *Curr. Med. Chem.*, 2010, **17**, 1255–1299.
15 F. Danhier, A. Le Breton, V. Préat, *Mol. Pharmaceutics*, 2012, **9**, 2961–2973.
16 R. Colombo, M. Mingozzi, L. Belvisi, D. Arosio, U. Piarulli, N. Carenini, P. Perego, N. Zaffaroni, M. De Cesare, V. Castiglioni, E. Scanziani, C. Gennari, *J. Med. Chem.*, 2012, **55**, 10460–10474.
17 M. Pilkington-Miksa, D. Arosio, L. Battistini, L. Belvisi, M. De Matteo, F. Vasile, P. Burreddu, P. Carta, G. Rassu, P. Perego, N. Carenini, F. Zunino, M. De Cesare, V. Castiglioni, E. Scanziani, C. Scolastico, G. Casiraghi, F. Zanardi, L. Manzoni, *Bioconjugate Chem.*, 2012, **23**, 1610–1622.
18 F. Bianchini, N. Cini, A. Trabocchi, A. Bottoncetti, S. Raspanti, E. Vanzi, G. Menchi, A. Guarna, A. Pupi, L. Calorini, *J. Med. Chem.*, 2012, **55**, 5024–5033.
19 L. Manzoni, L. Belvisi, D. Arosio, M.P. Bartolomeo, A. Bianchi, C. Brioschi, F. Buonsanti, C. Cabella, C. Casagrande, M. Civera, M. De Matteo, L. Fugazza, L. Lattuada, F. Maisano, L. Miragoli, C. Neira, M. Pilkington-Miksa, C. Scolastico, *ChemMedChem.*, 2012, **7**, 1084–1093.
20 J.-A. Park, Y.J. Lee, J.W. Lee, K.C. Lee, G.I. An, K.M. Kim, B.I. Kim, T.-J. Kim, J.Y. Kim, *ACS Med. Chem. Lett.*, 2014, **5**, 979–982.
21 L. Battistini, P. Burreddu, A. Sartori, D. Arosio, L. Manzoni, L. Paduano, G. D'Errico, R. Sala, L. Reia, S. Bonomini, G. Rassu, F. Zanardi, *Mol. Pharmaceutics*, 2014, **11**, 2280–2293.
22 H. Cai, P.S. Conti, *J. Label. Compd. Radiopharm.*, 2013, **56**, 264–279.
23 A. Eldar-Boock, K. Miller, J. Sanchis, R. Lupu, M.J. Vicent, R. Satchi-Fainaro, *Biomaterials*, 2011, **32**, 3862–3874.
24 D. Arosio, C. Casagrande, L. Manzoni, *Curr. Med. Chem.*, 2012, **19**, 3128–3158.
25 W. Lederle, M. Palmowski, F. Kiessling, *Curr. Pharm. Biotechnol.*, 2012, **13**, 595–608.
26 R. Chakravarty, H. Hong, W. Cai, *Curr. Drug Targets*, 2015, **16**, 592–609.
27 S.Y.A. Terry, M. Rijpkema, K. Abiraj, W.T. van der Graaf, W.J. Oyen, O.C. Boerman, *Curr. Pharm. Des.*, 2014, **20**, 2293–2307.
28 X. Lu, R.F. Wang, *Curr. Pharm. Des.*, 2012, **18**, 1032–1040.
29 R. Haubner, S. Maschauer, O. Prante, *BioMed. Res. Int.*, 2014, ID 871609.
30 Z. Liu, F. Wang, *Curr. Mol. Med.*, 2013, **13**, 1487–1505.
31 Y. Zhou, S. Chakraborty, S. Liu, *Theranostics*, 2011, **1**, 58–82.
32 J. Šimeček, J. Notni, T.G. Kapp, H. Kessler, H.-J. Wester, *Mol. Pharmaceutics*, 2014, **11**, 1687–1695.
33 H. Kolb, J. Walsh, J. Walsh, Q. Liang, T. Zhao, D. Gao, J. Secrest, L. Gomez, P. Scott, *J. Nucl. Med.*, 2009, **50** (Suppl 2), 329.

34 F.C. Gaertner, H. Kessler, H.-J. Wester, M. Schwaiger, A.J. Beer, *Eur. J. Nucl. Med. Mol. Imaging*, 2012, **39** (Suppl 1), S126–S138.

35 F. Zanardi, P. Burreddu, G. Rassu, L. Auzzas, L. Battistini, C. Curti, A. Sartori, G. Nicastro, G. Menchi, N. Cini, A. Bottoncetti, S. Raspanti, G. Casiraghi, *J. Med. Chem.*, 2008, **51**, 1771–1782.

36 L. Battistini, P. Burreddu, P. Carta, G. Rassu, L. Auzzas, C. Curti, F. Zanardi, L. Manzoni, E.M.V. Araldi, C. Scolastico, G. Casiraghi, *Org. Biomol. Chem.*, 2009, **7**, 4924–4935.

37 R. Varshney, P.P. Hazari, J.K. Uppal, S. Pal, R. Stromberg, M. Allard, A.K. Mishra, *Cancer Biol. Ther.*, 2011, **11**, 893–901.

38 A.J. Beer, R. Haubner, M. Goebel, S. Luderschmidt, M.E. Spilker, H.-J. Wester, W.A. Weber, M. Schwaiger, *J. Nucl. Med.*, 2005, **46**, 1333–1341.

39 S. Neubauer, F. Rechenmacher, A.J. Beer, F. Curnis, K. Pohle, C. D'Alessandria, H.-J. Wester, U. Reuning, A. Corti, M. Schwaiger, H. Kessler, *Angew. Chem. Int. Ed.*, 2013, **52**, 11656–11659.

40 A. Tolomelli, L. Gentilucci, E. Mosconi, A. Viola, S.D. Dattoli, M. Baiula, S. Spampinato, L. Belvisi, M. Civera, *ChemMedChem.*, 2011, **6**, 2264–2272.

41 D. Valdembri, G. Serini, *Curr. Opin. Cell. Biol.*, 2012, **24**, 582–91

42 S.D. Blystone, S.E. Slater, M.P. Williams, M.T. Crow, E.J. Brown, *J. Cell Biol.*, 1999, **145**, 889–897.

43 E. Vegt, M. Melis, A. Eek, M. de Visser, M. Brom, W.J. Oyen, M. Gotthardt, M. de Jong, O.C. Boerman, *Eur. J. Nucl. Med. Mol. Imaging*, 2011, **38**, 623–632.

44 J. Shi, Y. Zhou, S. Chakraborty, Y.-S. Kim, B. Jia, F. Wang, S. Liu, *Theranostics*, 2011, **1**, 322–340.

45 C. Decristoforo, I. Hernandez Gonzalez, J. Carlsen, M. Rupprich, M. Huisman, I. Virgolini, H.-J. Wester, R. Haubner, *Eur. J. Nucl. Med. Mol. Imaging*, 2008, **35**, 1507–1515.

46 Due to different experimental settings including type of xenografted tumor, injected dose, experiment time, data elaboration, a punctual comparison between in vivo results of **[111]In-2** and similar ^{111}In-labelled RGD ligands reported in the literature could not be carried out.

MedChemComm Accepted Manuscript

Graphical Abstract

Synthesis and Preclinical Evaluation of a Novel, Selective ^{111}In-labelled Aminoproline-RGD-peptide For Non-invasive Melanoma Tumor Imaging

Andrea Sartori, Francesca Bianchini, Silvia Migliari, Paola Burreddu, Claudio Curti, Federica Vacondio, Daniela Arosio, Livia Ruffini, Gloria Rassu, Lido Calorini, Alberto Pupi, Franca Zanardi and Lucia Battistini
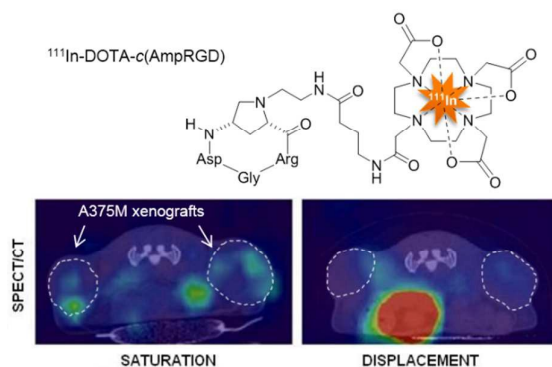
An ^{111}In-labelled Amp-based RGD-DOTA-conjugate was synthesized and evaluated in preclinical models of human melanoma as a novel integrin targeted SPECT imaging tracer.